Wear 332-333 (2015) 1314–1321

Contents lists available at ScienceDirect

Wear

journal homepage: www.elsevier.com/locate/wear

Effects of Pt cylinder arrays on macro-tribological properties of graphene and the SiO_2/Si substrate

H.Y. Wu [a,*], Z.B. Gu [b], Y. Lei [a], Q.F. Li [a], C.J. Gong [b], S.F. Shao [a], W.F. Rao [a]

[a] Department of Materials Physics, Nanjing University of Information Science and Technology, Nanjing 210044, China
[b] National Laboratory of Solid State Microstructures and Department of Materials Science and Engineering, Nanjing University, Nanjing 210093, China

ARTICLE INFO

Article history:
Received 3 September 2014
Received in revised form
30 January 2015
Accepted 4 February 2015

Keywords:
Cylinder arrays
Pt cylinders
Macro-tribological properties
Graphene
SiO_2/Si substrate

ABSTRACT

Hexagonal arrays of Pt cylinders with different diameters were prepared using magnetron sputtering technology onto SiO_2/Si substrates and also on graphene which was previously deposited onto a SiO_2/Si substrate. Friction and wear properties of different samples were investigated. The surface morphologies and composition at the center of the wear track were analyzed by scanning electron microscopy, Raman spectra and X-ray photoelectron spectroscopy. Results indicated that Pt cylinders with different diameters acted as very strong pinning centers for the sliding of graphene sheets, and affected the subsequent friction. The higher the Pt surface coverage, the stronger the effect of Pt cylinders on the lubrication performance. As such, the friction and wear of large-diameter Pt cylinders on graphene and the SiO_2/Si substrate were more effective in reducing the friction. On the contrary, for small-diameter Pt cylinders, the interaction between graphene and Pt cylinders played a key role in the improvement of macro-tribological properties. Overall, the Pt cylinders played an important lubrication role on the friction and wear. Graphene introduced as an adhesion layer between Pt cylinders and the SiO_2/Si substrate could support both deformed and undeformed Pt cylinders.

1. Introduction

Micro-electromechanical systems (MEMS) have extremely low tolerance for friction and wear since even the smallest wear particles could cause seizure and catastrophic failure [1,2]. Graphene, as the thinnest solid lubricant, exhibits superior properties, including chemical stability even under extreme environmental conditions and, when stacked in a lamellar structure, low shear strength similar to graphite [3,4]. Recent mechanical experiments have shown that graphene is the strongest material measured so far [5,6]. However, the friction and wear lifetime problems induced by the strong surface adhesion of graphene have severely restricted the future applications of MEMS.

Both the surface hydrophobic property and the real contact area are two key factors for decreasing friction and adhesion of MEMS devices [7]. Graphene has a large theoretical specific surface area (2630 $m^2 g^{-1}$), which imparts its special surface characteristics [8]. Graphene surface has different absorption in the friction process, which prevents the formation of transferred films. It leads to an increase in the friction coefficient and reduces the wear lifetime. As has been reported in our previous research [9], CVD-grown graphene exhibits a low friction coefficient, but the wear-proof lifetimes were much shorter than that in the literature [10]. They proposed that the assembled reduced graphene oxide (RGO) applied to MEMS/NEMS devices could be used as a lubricant for reducing the friction coefficient and prolong the wear-proof lifetimes.

In view of the above discussion, the surface micro-texture of materials is crucial for controlling the surface composition, structure and interfacial properties to minimize the friction and prolong wear-proof lifetimes. The mechanism is reported to be the introduction of a thin lubricant film [11,12]. Platinum (Pt) would appear to be a suitable material for tribological applications due to its low hardness and notable environmental stability [13]. Being different from other materials, Pt cylinders supported on graphene will exhibit unique macro-tribological properties. It is due to the fact that graphene can improve the adhesion of Pt to substrates (e.g. Si or SiO_2). As has been reported previously [14,15], the growth mechanisms of a few layers of graphene are based on layer by layer growth. The layer-by-layer stacking of continuous graphene sheets reduces the coupling between adjacent graphene layers. Research demonstrated [16] that the interactions between a Pt (111) surface and graphene could be enhanced due to the effects of carbon vacancies on the graphene sheets. Also, the interface became more stable as the number of Pt atoms increased the three-dimensional planar configurations. In addition, the interconnected flexible network of graphene has a certain cohesive energy with the SiO_2/Si substrate due to the existence of the oxygen defects in the SiO_2 surface [17]. Our previous research had also found that the Pt cylinder-array structures on the graphene surface prevented the folding effect, induced by the relative sliding between layers and large-scale curling of graphene sheet

* Corresponding author.
E-mail address: whyc3w3@126.com (H.Y. Wu).

http://dx.doi.org/10.1016/j.wear.2015.02.041
0043-1648/

edge, and therefore prolonged the wear lifetime of the graphene. The results indicated that Pt cylinders have an influence on both the macro-tribological properties of graphene and on the SiO_2/Si substrate. Graphene, as an adhesion layer, had not only a significant influence on mechanical properties, but improved also the adhesive strength between the SiO_2/Si substrate and Pt cylinders. However, it is not clear that the Pt cylinder arrays affect the macro-tribological properties of the SiO_2/Si substrate and graphene.

The aim of the present study was to determine the effects of different size Pt cylinder-array structures on macrotribological properties of the SiO_2/Si substrate and graphene. Hexagonal arrays of Pt cylinders with different diameters were prepared on a graphene–covered SiO_2/Si substrate (Pt/graphene) and directly on a SiO_2/Si substrate (Pt/SiO_2), using a metal mask method and magnetron sputtering technology, respectively. We investigated the friction and wear properties of Pt/graphene and Pt/SiO_2 with different diameters of Pt cylinders, resulting in different area coverages. The findings are expected to provide an effective way to expand the future applications of graphene in macro-tribological properties of micro-electromechanical systems.

2. Material and methods

2.1. Sample preparation

Graphene was prepared on Cu foils ($20 \times 20 \times 0.025$ mm^3) by CVD in a 5-inch quartz tube. While the furnace was heated from room temperature to 1000 °C, H_2 (10 sccm) gas flow cleaned and reduced the Cu catalyst for 30 min. CH_4 (65 sccm) flowed for 15 min to generate a carbon source at 1000 °C. Then, the furnace was quickly cooled to below 400 °C under an H_2 gas atmosphere. After graphene was grown on Cu foils, poly (methyl methacrylate) (PMMA) was used as a supporting layer to protect the synthesized graphene during the etching process. The Cu catalyst was removed by 0.5 mol/L ferrous trichloride solution, $FeCl_3$ for 3 h, followed by de-ionized water rinsing. PMMA/graphene membranes were transferred onto the Si wafer ($15 \times 15 \times 2$ mm^3) with a 300 nm-thick SiO_2 layer (graphene/SiO_2/Si), which was similar to a previously reported process [18]. The PMMA supporters were removed by dipping the sample in acetone at 80 °C to minimize the PMMA residue.

We fabricated a periodic array of Pt cylinders with different diameters on the graphene and on the SiO_2/Si substrate by the shadow mask method using magnetron sputtering technology. The metal shadow mask with a hexagonal-array of holes was laid on the top of graphene surface. Three different sizes of Pt cylinders were investigated. One with small-diameter cylinders (Φ100 μm × 100 nm), the second with large-diameter cylinders, (Φ250 μm × 100 nm) and the third with mixed large- and small-diameters arranged on the graphene (designated S-Pt/graphene, L-Pt/graphene, and LS-Pt/graphene, respectively). Identical arrays of platinum cylinders were also deposited directly on SiO_2/Si substrates, designated S-Pt/SiO_2, L-Pt/SiO_2, and LS-Pt/SiO_2, respectively. The surface micro-textures were also modeled as hexagonal arrays of Pt cylinders with different diameters.

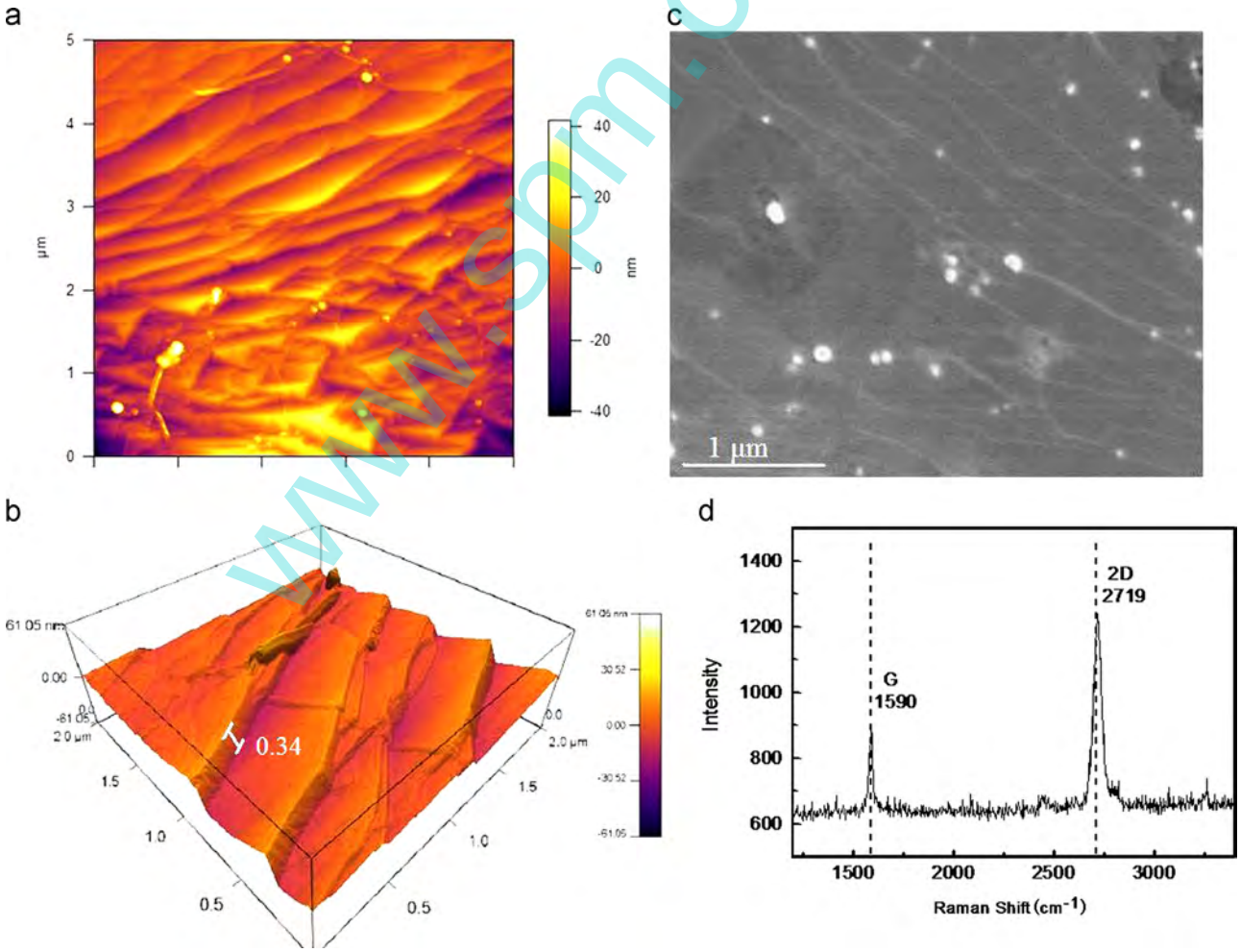

Fig. 1. (a) AFM surface morphologies of CVD-grown graphene on Cu foils, (b) 3-D profile showing the step-edge in-plane growth and (c) scanning electron microscopy image and (d) Raman spectrum of graphene transferred on the SiO_2/Si substrate.

2.2. Microstructure analysis and macro-tribological properties

The surface morphologies of graphene were characterized by scanning electron microscopy (SEM, JEOL JSM-6300) and an atom force microscope (AFM, CSPM4000). Raman spectra (Labram HR800 Jobin Yvon) were also employed to analyze the microstructure of the samples using a 514-nm laser excitation. The mean value of three repetitive measurements for each sample from different areas was obtained. X-ray photoelectron spectroscopy (XPS, K-alpha) was performed using monochromatic Al Kα irradiation.

Macro-tribological tests were run on a UMT-2MT tribometer (Bruker) in a ball-on-plate contact configuration under the testing conditions of 0.1 N, 0.5 cm stroke length, at a frequency of 1 Hz. GCr15 steel balls (6 mm diameter, mean roughness is 0.02 μm) were used as the stationary upper counterparts, and the lower tested samples were mounted onto the flat base and were driven to slide reciprocally. The friction-coefficient-versus-time curves were generated automatically. All experiments were performed under ambient conditions of 25 °C and 26% relative humidity.

3. Results and discussion

3.1. Microstructure and Raman characterization of CVD-grown graphene

The surface morphologies of CVD-grown graphene on Cu foils and the SiO_2/Si substrate were examined by SEM and AFM, typical results are shown in Fig. 1. As shown in Fig. 1(a), AFM analysis shows the step-edge in-plane growth of graphene on Cu foil, which is consistent with the recent report by Liu et al. [19]. It is revealed that the orientation of the growth is strongly influenced by the step-edge structure. Also, the thickness of the step-edge in-plane growth corresponds to the theoretical value of 0.34 nm for a perfectly flat sp^2-carbon-atom network, as illustrated in Fig. 1(b). Meanwhile, the microstructure of the graphene/SiO_2/Si is shown in Fig. 1(c). It is interesting to note that the layer-by-layer feature of graphene can be clearly observed. A continuous uniform graphene was transferred onto the SiO_2/Si substrate.

Raman spectrum of the graphene/SiO_2/Si is shown in Fig. 1(d). Typical G and 2D bands are observed at ~1580 and 2700 cm^{-1}, respectively. The intensity ratio of 2D/G peaks is 1.6, which corresponds to that of a few-layered graphene [21]. The ratio of 2D/G peaks is related to the degree of recovery for sp^2 C=C bonds (graphitization) in the graphitic structure [22].

3.2. Modeling of hexagonal arrays of Pt cylinders with different diameters

The schematic diagrams of Pt cylinders with different diameters are illustrated in Fig. 2. The surface micro-textures of the graphene/SiO_2/Si and SiO_2/Si are modeled as hexagonal arrays of circular cylinders of uniform diameter (d) distributed with a certain coverage (V_d) (the Pt surface coverage per unit area). The center-to-center distance from a particular cylinder to its nearest neighbor is denoted by L, as illustrated in Fig. 2(a). V_d as a function of cylinder radii (R or r) is given as

$$V_d = \frac{2(4\pi R^2 + 5\pi r^2)}{9\sqrt{3}L^2} \text{ or } \frac{2(4\pi r^2 + 5\pi R^2)}{9\sqrt{3}L^2},$$

where L is a constant (~375 μm), R and r are large-scale and small-scale diameters, respectively. When R is equal to r, V_d corresponds to V_L or V_S. Herein, V_L, V_{L-S} and V_S are referred to as the Pt surface coverage with large-scale, large- and small-scale and small-scale diameters, respectively. They are 58.1%, 31% and 9.3%, respectively. It can be noted that L-Pt/graphene and L-Pt/SiO_2 have the highest Pt surface coverage, and V_{L-S} is between V_L and V_S, as illustrated in Fig. 2(b) and (c). It can be expected that the higher the Pt surface coverage is, the stronger the effect of Pt cylinders on the lubrication performance will be. The size effect of the Pt cylinders affects the Pt surface coverage, which plays a crucial role in decreasing the coefficient of friction (COF) during sliding.

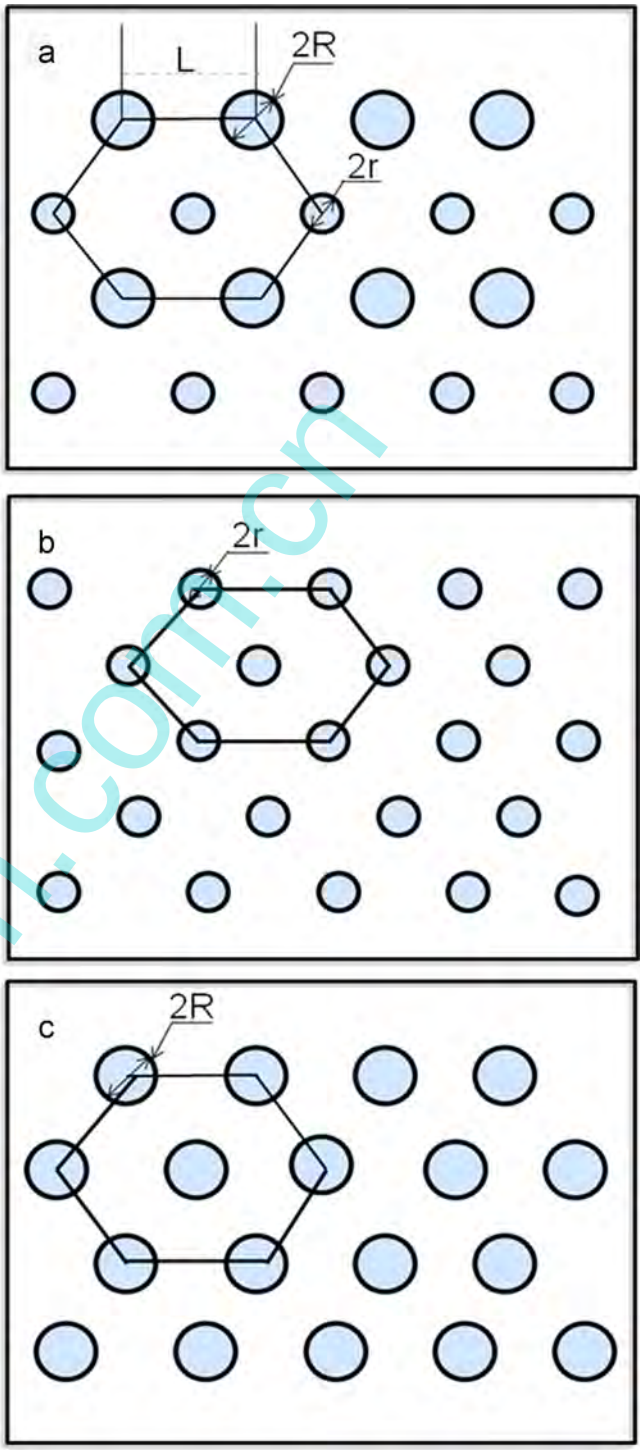

Fig. 2. The schematic diagrams of Pt cylinders with (a) large- and small-scale, (b) small-scale and (c) large-scale diameters. L was approximately 375 μm.

Additionally, when Pt cylinders are supported on graphene, carbon vacancies on a graphene sheet can enhance the Pt–graphene interaction [23], just as the Pt cylinders pin the graphene sheets. The cylinder arrays form some geometrical configurations, which appear an integer number of pins per unit cell of the regular

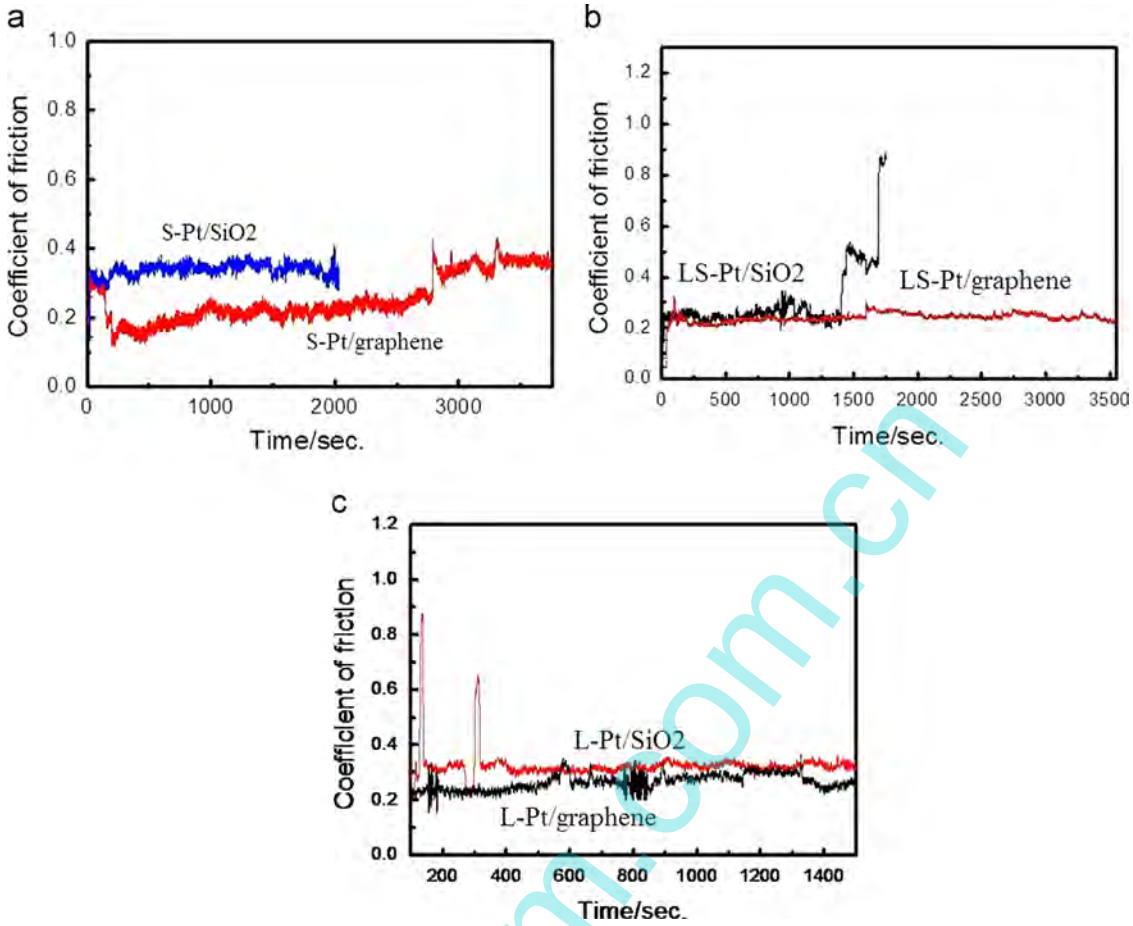

Fig. 3. The coefficients of friction of the hexagonal arrays of Pt cylinders with different diameters arranged on the SiO_2/Si substrate and graphene. The comparison of (a) S-Pt/SiO_2 and S-Pt/graphene, (b) LS-Pt/SiO_2 and LS-Pt/graphene, and (c) L-Pt/SiO_2 and S-Pt/graphene, respectively.

array [24]. The pinning centers density of the array corresponds to V_d. As discussed previously, the artificial regular array acts as very strong pinning centers for the sliding of graphene sheets. The large-diameter Pt cylinders has a bigger contact area than the small diameter, therefore the former has a stronger pinning effect than the latter. Due to the poor adhesion between Pt and SiO_2 [25], the pinning effect of Pt/SiO_2 is different from Pt/graphene. When there is no graphene present, there may be sliding at the interface between the Pt cylinders and the SiO_2 film and the wear lifetime of Pt/SiO_2 may be shorter than that of Pt/graphene.

3.3. *Effect of Pt cylinders with different diameters on the friction and wear of graphene and SiO_2/Si*

Results of the ball-on-plate friction and wear tests are shown in Fig. 3, in which the COFs of S-Pt/SiO_2, LS-Pt/SiO_2 and L-Pt/SiO_2 are compared with those of S-Pt/graphene, LS-Pt/graphene and L-Pt/graphene. In Fig. 3(a), the S-Pt/SiO_2 has an average friction coefficient of 0.30. The COF of S-Pt/graphene is approximately 0.20 up to 2800 s, after which it increases to 0.30. This indicates that graphene introduced between Pt cylinders and the SiO_2/Si substrate is beneficial for decreasing the COF. Fig. 3(b) displays the COFs of the LS-Pt/SiO_2 and the LS-Pt/graphene against steel balls. LS-Pt/SiO_2 exhibits a very stable range of friction coefficient (0.20–0.25) under the load of 0.1 N, and has the same friction coefficient as the LS-Pt/graphene before 1300 s, and then the COF of the former sharply increase to 1.0, indicating wear-through to the Si substrate. The results show that the wear-proof lifetime of the LS-Pt/graphene (>3500 s) is more than twice that of the LS-Pt/SiO_2 ($\sim$1300 s). As shown in Fig. 3(c), L-Pt/SiO_2 and the L-Pt/graphene display similar low-friction values, while the latter has slightly lower COF. It can also be seen that the COF of the L-Pt/SiO_2 presents two severe fluctuations at the first stage. This may be a result of the poor adhesion of Pt cylinders to silicon and silicon dioxide surfaces. Because the L-Pt/SiO_2 and the L-Pt/graphene are covered by a greater area fraction of Pt cylinders, the Pt cylinders with the large-scale diameter will likely provide more wear debris than the other two. When more Pt cylinders participate in the sliding contact, the low shear strength of Pt reduces the friction between Pt and steel. Hence, Pt can be a lubricating medium and acts as "the third body" between graphene and the steel counterface to avoid the scaling of graphene sheets from the SiO_2/Si substrate. The role of wear debris depends on the amount of the spoiled Pt cylinders. In view of above discussion, Pt cylinders have an important influence on the frictional properties of the SiO_2/Si substrate and graphene.

To further explore the size effects of Pt cylinders on the macro-tribological properties, the worn surface morphologies, composition and surface structure on the wear track were analyzed by conducting SEM and obtaining Raman spectra.

Fig. 4 shows the worn morphologies of the Pt/graphene and Pt/SiO_2 with the small-diameter, large-diameter and large- and small-diameter cylinder. It can be seen from Fig. 4(a), (c) and (e) that the Pt cylinders and SiO_2 film are worn under the contact and deep grooves were formed, which terminated at the end of the stroke, where the wear debris was deposited. Because the wear debris is mainly caused by the worn Pt cylinders, indicated in Fig. 6, the S-Pt/SiO_2 produces the least wear debris among them, as indicated in Fig. 4 (a). Similarly, in Fig. 4(c) and (e), the LS-Pt/SiO_2 and the L-Pt/SiO_2 generate more wear debris. Fig. 4(b), (d) and (f) shows the worn

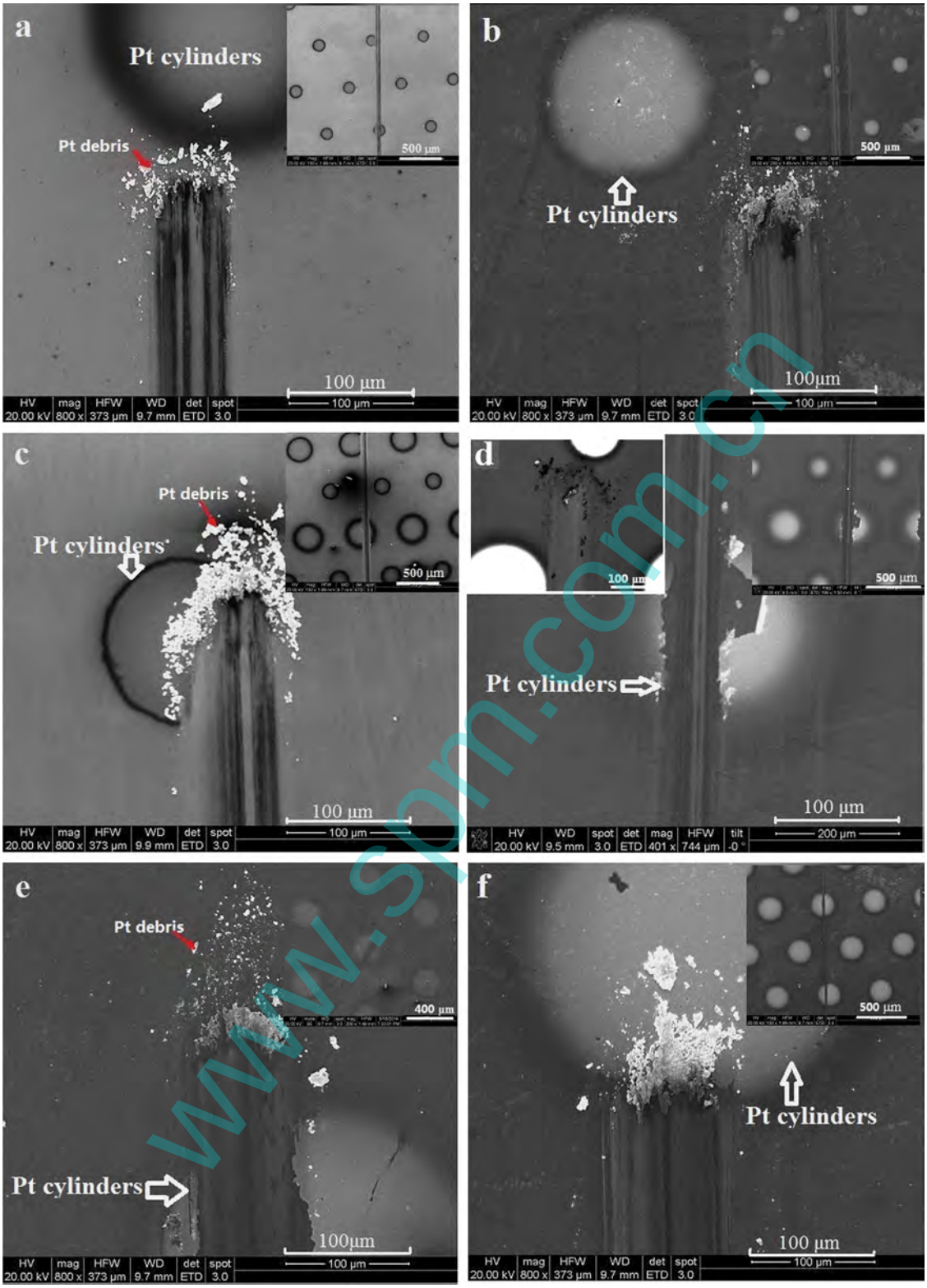

Fig. 4. The worn morphologies of Pt/SiO_2 and Pt/graphene with small-scale, large- and small-scale and large-scale diameters under the load of 0.1 N. (a) S-Pt/SiO_2, (b) S-Pt/graphene, (c) LS-Pt/SiO_2, (d) LS-Pt/graphene, (e) L-Pt/SiO_2 and (f) L-Pt/graphene, respectively. The circular objects are the Pt cylinders.

surface morphologies of the S-, LS- and L-Pt/graphene samples respectively. Fig. 4(b) and (d) shows that the smooth and very shallow wear tracks are present on the S-Pt/graphene and the LS-Pt/graphene, and their wear debris do not produce the noticeable exfoliations. On the contrary, we can clearly find in Fig. 4(f) that the L-Pt/graphene shows deeper plowing than the other two and formed amount of wear debris which are commonly flake-like, corresponding to a soft film (Pt) on hard substrates (the graphene/SiO_2/Si). For the Pt/graphene systems, although the thickness of graphene is negligible because it is less than 1 nm, its mechanical effects should not be overlooked. According to a study reported by Xin et al., graphene is a promising supporting material due to its high compressive strength

[26]. When the indenter comes into contact with graphene, the carbon network of graphene will provide a thin support layer for Pt cylinders until the frame is broken. Therefore, graphene could effectively supports the Pt cylinders in the friction and wear. It can be accompanied by the analysis of Raman spectra at the center of the wear track, as shown in Fig. 5.

Fig. 5(a) shows Raman spectra of the S-, LS-, and the L-Pt/SiO_2 at the center of the wear track after the friction tests. It is observed at ~520 cm^{-1} and ~960 cm^{-1} in the Raman spectra of the typical Si structure, which is consistent with the SiO_2/Si substrate before the friction test. It illustrates that Pt cylinders are completely extruded on two sides of the wear track, as well as at the ends of the track, and there is no obvious Pt wear debris observed in the wear track. For Pt/SiO_2, Pt debris cannot be observed in the wear track and they will accumulate outside of the track due to the poor adhesion between Pt and SiO_2. Raman spectrum of wear debris exhibits a weak peak at 520 nm (Si), indicating stronger absorption in the thicker Si or SiO_2 debris. By contrary, Raman spectra of S-Pt/graphene, LS-Pt/graphene and L-Pt/graphene indicate that there are obvious D band and G bands at the center of the wear track (from Fig. 5(b)). These are interpreted to be a disordered D band, located around 1345 cm^{-1}, and an active graphite G band, located around 1602 cm^{-1}. The ratio of the intensity

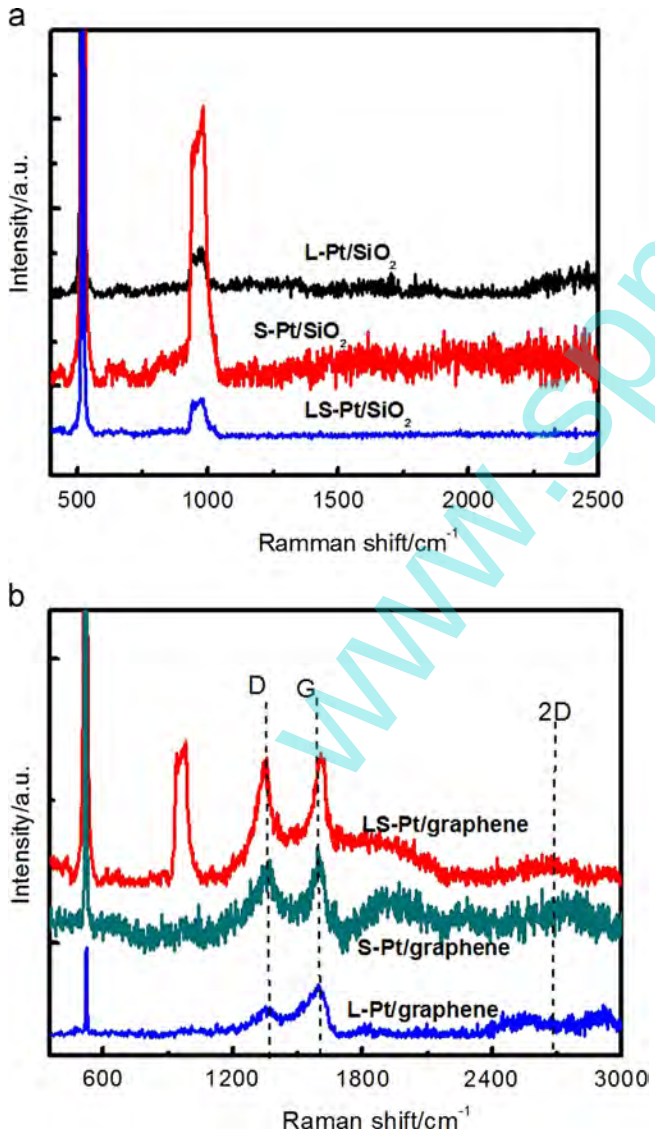

Fig. 5. Raman spectra of (a) Pt/SiO_2 and (b) Pt/graphene with different diameters at the center of the wear track after the friction tests.

of a D band to that of a G band (I_d/I_g) is related to the microstructure changes of the graphene surface because it correlates with the sp^3/sp^2 bonding ratio and the size of graphite clusters [27]. The smaller I_d/I_g peak intensity ratio of the Raman spectrum indicates lower defects and disorders of the graphitized structures containing the disorders caused at the edges of the carbon platelets. It is calculated that the intensity ratio of I_d/I_g is around 1.5, 1.1, 0.6 and 0.7 for the S-Pt/graphene, the LS-Pt/graphene, the L-Pt/graphene and the Pt/graphene, respectively. It can be seen that the L-Pt/graphene has little influence on the graphitized structures due to graphene covered by a large amount of the worn Pt film. Compared to D and G bands of graphene, Raman spectra of three samples display obvious asymmetrical D and G bands in the wear track, indicating that sp^2-hybridized carbon is affected by the friction process. Additionally, it is noticeable that weak 2D bands at ~2700 cm^{-1} are present in the wear track of the S-Pt/graphene and the LS-Pt/graphene, while there is no existence of 2D band for the L-Pt/graphene. 2D band is always observed in graphite samples, which is regarded as a function of the number of layers. A further increase of the number of layers leads to a significant decrease of the relative intensity of the lower frequency 2D peaks. For graphene with more than five layers, Raman spectra become hardly distinguishable from those of bulk graphite. It can be deduced that the folds and carbonation degree of the Pt/graphene increase as the friction proceeds. As the diameter of Pt cylinders increases, the role of Pt in the friction and wear between graphene and steel is expanding.

According to the above discussion, we can clearly find that graphene for different diameters cylinders is not easily extruded to the sides of the wear track. As the diameter of Pt cylinders is decreased, the effect of graphene on the macro-tribological properties is more obvious than that of Pt cylinders. Due to its high compressive strength, graphene introduced as an adhesion layer between Pt and SiO_2/Si can support soft Pt cylinders, and plays an effective support role in the friction.

In order to reveal effect of the interaction between graphene and Pt on macro-tribological properties, it is necessary to investigate the composition and bonding states of the wear debris by XPS.

Fig. 6 shows XPS spectra of elements presented in wear debris of the LS-Pt/SiO_2 and the LS-Pt/graphene. After the friction test, as indicated in Fig. 6(a), XPS spectra of Pt 4f in the LS-Pt/SiO_2 display the presence of two pairs of doublets with binding energies of 71.3 (Pt, 4f7/2) and 74.5 eV (Pt, 4f5/2), which is attributed to metallic Pt [28]. It is indicated that Pt cylinders exhibit a weak cohesion with the SiO_2/Si substrate due only to van der Waals forces [26]. On the contrary, in Fig. 6(b), the deconvolution of the Pt shows peaks at 72.1 eV (Pt 4f7/2) and 75.6 eV (Pt 4f5/2) could be attributed to $Pt^{\delta+}$, that anchored with the C–O group. It can be deduced from XPS analysis that a strong interaction among Pt, C, and SiO_2 film are present in the Pt/graphene system when graphene as an adhesion layer is introduced between Pt cylinders and the SiO_2/Si substrate.

3.4. *Macro-tribological mechanisms of Pt cylinder arrays on graphene and the SiO_2/Si substrate*

To discuss the macro-tribological mechanisms of the Pt/SiO_2 and the Pt/graphene against the steel counterface, the schematic diagrams of the friction tests are shown in Fig. 7. Fig. 7(a) and (b) illustrates the Pt cylinder-array structure supported on the graphene and the SiO_2/Si substrate, respectively. The steel counterface can direct contact the large or small diameter Pt cylinders. Due to the presence of Pt cylinders, there are sharply decreasing in friction coefficient, compare to the samples without Pt cylinders. It also indicates that Pt cylinder arrays have obvious effects on the lubrication performance of the graphene and SiO_2/Si surface. Therefore, in the initial stage of the friction, Pt cylinders can prevent the indenter from direct contact with the graphene and the SiO_2/Si surface before Pt was rubbed off from the cylinder, shown in Fig. 7(c) and (d). As the

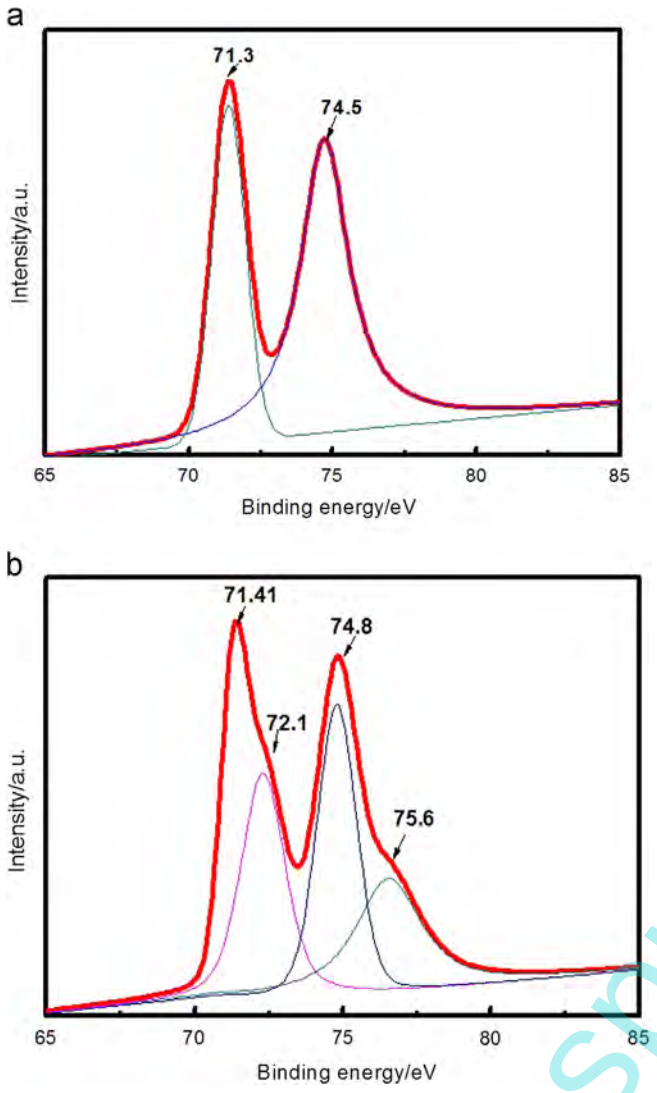

Fig. 6. XPS spectra of Pt 4f present in the wear debris of (a) LS-Pt/SiO_2 and (b) LS-Pt/graphene.

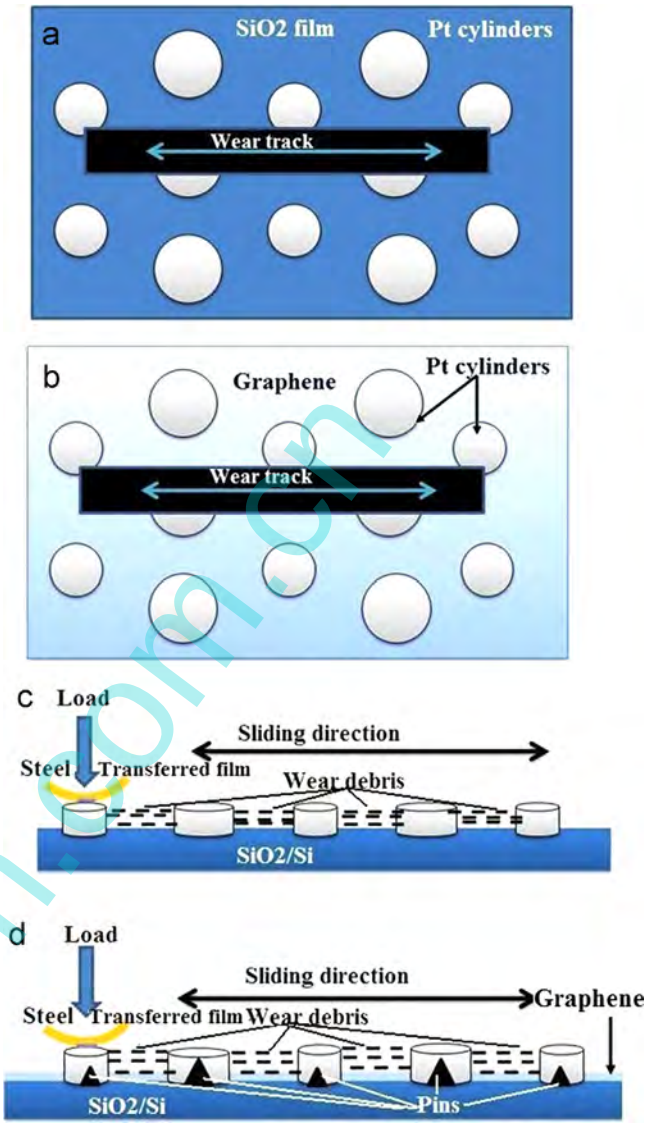

Fig. 7. The schematic illustrations of the arrays of Pt cylinders on (a) graphene and (b) SiO_2/Si, and schematic diagrams of the friction tests of (c) Pt/SiO_2 and (d) Pt/graphene against the steel counterface.

Pt cylinder arrays were rubbed, due to its low hardness, Pt is not enough to bear the load so that it is easily plowed or destroyed. Pt partly transferred to the steel counterface, which will be partly covered with Pt film. The low shear strength of Pt reduces the friction between Pt and steel counterface. Pt can be a lubricating medium and acts as "the third body" between steel and counterface materials (e.g. the graphene/SiO_2/Si and the SiO_2/Si substrate).

As the test duration further increases and Pt cylinders are plowed or destroyed, the steel counterface has the chance to directly contact the SiO_2/Si substrate, as shown in Fig. 7(c). As for the Pt/graphene, Pt cylinders act like pins and prevent the graphene from sliding between the Pt and SiO_2/Si substrate, marked by the triangles region shown in Fig. 7(d). The cylinder arrays act as very strong pinning centers for the sliding of graphene sheets. The larger the diameter of Pt cylinders, the stronger the pinning effect. After Pt cylinders are worn, graphene due to its high compressive strength, introduced as an adhesion layer between Pt cylinders and the SiO_2/Si substrate, can support the worn and unworn Pt cylinders. The sliding occurs between graphene and the steel counterface partly covered with Pt. At this moment, the surface states of graphene greatly changed, including defects and composition. Graphene directly contacted with the steel counterface can cause the grain boundary motion and the formation of defects. Alternatively, the oxidation of the graphene surface can be induced, further decreasing its surface energy and wear resistance.

Therefore, Pt cylinders are supported on the graphene surface to keep a strong adhesion to the SiO_2/Si substrate. The interaction between Pt cylinders and graphene is beneficial for decreasing the friction coefficient and prolonging the wear-proof lifetimes.

4. Conclusions

We prepared hexagonal arrays of Pt cylinders with different diameters on SiO_2/Si substrates and on graphene/SiO_2/Si using magnetron sputtering. The results indicated that the friction and wear of the large-diameter Pt cylinders on the SiO_2/Si substrate and on the graphene/SiO_2/Si sample were affected mainly by the lubrication due to the Pt cylinders. As for the Pt/graphene/SiO_2/Si systems, no matter what the sizes of the cylinders were, graphene, which was introduced as an adhesion layer between Pt cylinders and the SiO_2/Si substrate and can support the worn and unworn Pt cylinders. Pt cylinders act as a series of pins, preventing the graphene from sliding between the Pt cylinders and the SiO_2/Si substrate. Therefore, the

interaction between graphene and Pt cylinders plays a crucial role in the improvement of macro-tribological properties.

Acknowledgments

This project is supported by National Natural Science Foundation of China (Grant nos. 51405242, 51245010, and 11047143), Natural Science Foundation of Jiangsu Province of China (Grant no. BK2012463).

References

[1] J.J. Rha, S.C. Kwon, J.R. Cho, S. Yim, N. Sak, Creation of ultra-low friction and wear surfaces for micro-devices using carbon films, Wear 259 (2005) 1–6.
[2] S. Tadigadapa, N. Najafi, Reliability of micro-electro-mechanical systems (MEMS), J. Microelectromech. Syst. 11 (2002) 206–214.
[3] C.G. Lee, Q.Y. Li, W. Kalb, X.Z. Liu, H. Berger, R.W. Carpick, J. Hone, Frictional characteristics of atomically thin sheets, Science 328 (2010) 76–80.
[4] K.-S. Kim, H.-J. Lee, C.G. Lee, S.-K. Lee, H. Jang, J.–H. Ahn, J.–H. Kim, H.-J. Lee, Chemical vapor deposition-grown graphene: the thinnest solid lubricant, ACS Nano 5 (2011) 5107–5114.
[5] K. Min, N.R. Alurua, Mechanical properties of graphene under shear deformation, Appl. Phys. Lett. 98 (2011) 0131131–0131133.
[6] F. Scarpa, S. Adhikari, A.S. Phani, Effective elastic mechanical properties of single layer graphene sheets, Nanotechnology 20 (2009) 065709–065720.
[7] Y.C. Jung, B. Bhushan, Contact angle, adhesion and friction properties of micro- and nanopatterned polymers for superhydrophobicity, Nanotechnology 17 (2006) 4970–4980.
[8] S. Wang, Y. Zhang, N. Abidi, L. Cabrales, Wettability and surface free energy of graphene films, Langmuir 25 (2009) 11078–11081.
[9] H.Y. Wu, Z.B. Gu, C.J. Gong, Y. Lei, D. Mo, S.T. Zhang, Y.B. Chen, Y.F. Chen, Macrotribological behavior of the graphene surface structured in a cylinder array, Surf. Coat. Technol. 236 (2013) 296–302.
[10] J.F. Ou, J.Q. Wang, S. Liu, B. Mu, J.F. Ren, H.G. Wang, S.R. Yang, Tribology study of reduced graphene oxide flakes on silicon substrate synthesized via covalent assembly, Langmuir 26 (2010) 15830–15836.
[11] A. Ramesh, W. Akram, S.P. Mishra, A.H. Cannon, A.A. Polycarpou, W.P. King, Friction characteristics of microtextured surfaces under mixed and hydrodynamic lubrication, Tribol. Int. 57 (2013) 170–176.
[12] D. Xiong, Y. Qin, J. Li, Y Wan, R Tyagi, Tribological properties of PTFE/laser surface textured stainless steel under starved oil lubrication, Tribol. Int. 82 (2015) 305–310.
[13] N.W. Khun, E. Liu, Effects of platinum content on tribological properties of platinum/nitrogen doped diamond-like carbon thin films deposited via magenetraon sputtering, Friction 2 (2014) 64–72.
[14] Y.P. Wu, H. Chou, H.X. Ji, Q.Z. Wu, S.S. Chen, W. Jiang, Y.F. Hao, J.Y. Kang, Y.J. Ren, Richard D. Piner, Rodney S. Ruoff, Growth mechanism and controlled synthesis of AB-stacked bilayer graphene on Cu–Ni alloy foils, ACS Nano 6 (2012) 7731–7738.
[15] R. Negishi, H. Hirano, Y. Ohno, K. Maehashi, K. Matsumoto, Y. Kobayashi, Layer-by-layer growth of graphene layers on graphene substrates, Thin Solid Films 519 (2011) 6447–6452.
[16] F.G. Sen, Y. Qi, A.T. Alpas, Anchoring platinum on graphene using metallic adatoms: a first principles investigation, J. Phys.: Condens. Matter 24 (2012) 25003–250014.
[17] K.O. Maeda, Y. Morikawa, S. Tanaka, M. Kohyama, Structures of Pt clusters on graphene by first-principles calculations, Surf. Sci. 604 (2010) 144–154.
[18] C. Mattevi, H. Kim, M. Chhowalla, A review of chemical vapour deposition of graphene on copper, J. Mater. Chem. 21 (2011) 3324–3334.
[19] Z. Liu, Y.-C. Lin, C.-C. Lu, C.-H. Yeh, P.-W. Chiu, S. Iijima, K. Suenaga, In situ observation of step-edge in-plane growth of graphene in a STEM, Nat. Commun. 5 (2014) 1–7.
[21] D. Graf, F. Molitor, K. Ensslin, C. Stampfer, A. Jungen, C. Hierold, L. Wirtz, Spatially resolved Raman spectroscopy of single- and few-layer graphene, Nano Lett. 7 (2007) 238–242.
[22] Y.C. Lin, K.K. Liu, C.Y. Wu, C.W. Chu, J.W. Wang, C.T. Liang, L.J. Li, Efficient reduction of graphene oxide catalyzed by copper, Phys. Chem. Chem. Phys. 14 (2012) 3083–3088.
[23] F.G. Sen, Y. Qi, A.T. Alpas, Anchoring platinum on graphene using metallic adatoms: a first principles investigation, J. Phys.: Condens. Matter 24 (2012) 225003–2250015.
[24] R. Cao, H. Lance, J.C. Wu, T.J. Yang, T.C. Wu, Pinning effects in Nb thin films with artificial pinning array, J. Supercond. Nov. Magn. 23 (2010) 1051–1054.
[25] A. Ababneh, A.N. Al-Omari, M. Marschibois, D. Feili, H. Seidel, Investigations on the high temperature compatibility of various adhesion layers for platinum, Proc. Spie 8763 (2013) 1–6.
[26] Y.C. Xin, J.G. Liu, Y. Zhou, W.M. Liu, J. Gao, Y. Xie, Y. Yin, Z.G. Zou, Preparation and characterization of Pt supported on graphene with enhanced electrocatalytic activity in fuel cell, J. Power Sources 196 (2011) 1012–1018.
[27] A.C. Ferrari, Raman spectroscopy of graphene and graphite: disorder, electron–phonon coupling, doping and nonadiabatic effects, Solid State Commun. 143 (2007) 47–57.
[28] R.F. Nie, J.H. Wang, L. Wang, Y. Qin, P. Chen, Z.Y. Hou, Platinum supported on reduced graphene oxide as a catalyst for hydrogenation of nitroarenes, Carbon 50 (2012) 586–596.